Investigation and Simulation of Diffraction on Rough Surfaces

O. Clausen,[1,2] Y. Chen,[3] A. Fuhrmann[1] and R. Marroquim[3]

[1]TH Köln, Köln, Germany
[2]Federal University of Rio de Janeiro, Rio de Janeiro, Brazil
[3]Delft University of Technology, Delft, The Netherlands

Abstract

Simulating light–matter interaction is a fundamental problem in computer graphics. A particular challenge is the simulation of light interaction with rough surfaces due to diffraction and multiple scattering phenomena. To properly model these phenomena, wave-optics have to be considered. Nevertheless, the most accurate BRDF models, including wave-optics, are computationally expensive, and the resulting renderings have not been systematically compared to real-world measurements. This work sheds more light on reflectance variations due to surface roughness. More specifically, we look at wavelength shifts that lead to reddish and blueish appearances. These wavelength shifts have been scarcely reported in the literature, and, in this paper, we provide the first thorough analysis from precise measured data. We measured the spectral in-plane BRDF of aluminium samples with varying roughness and further acquired the surface topography with a confocal microscope. The measurements show that the rough samples have, on average, a reddish and blueish appearance in the forward and back-scattering, respectively. Our investigations conclude that this is a diffraction-based effect that dominates the overall appearance of the samples. Simulations using a virtual gonioreflectometer further confirm our claims. We propose a linear model that can closely fit such phenomena, where the slope of the wavelength shifts depends on the incident and reflection direction. Based on these insights, we developed a simple BRDF model based on the Cook–Torrance model that considers such wavelength shifts.

Keywords: rendering, reflectance & shading models, diffraction

CCS Concepts: • Computing methodologies → Reflectance modelling

1. Introduction

In computer graphics, the simulation of light–matter interaction is a major challenge. Often, it is described by the bidirectional reflectance distribution function (BRDF). Even though there are different ways to define the material's BRDF, a physically based analytical formulation is commonly preferred. These BRDFs are based on physical parameters and model the surface reflectance in a physically plausible manner.

Analytical BRDFs are designed using real-world observations or physical measurements and are usually based on geometric optics. BRDF databases, such as the well-known MERL [MPBM03] and UTIA [FVH14, FV14], are crucial to pushing forward research in the field. Nevertheless, these databases are not free of drawbacks making a sound analysis and modelling of light–matter interaction hard or, in some situations, even impossible. For the MERL and UTIA datasets, for example, the whole light spectrum is represented by RGB triplets, complicating modelling wavelength-dependent scattering phenomena.

Current BRDF models based on geometric optics lead to photorealistic images but often fail to be predictive [NDM05, BNM15, YHW*18], especially for rough surfaces. Such surfaces contain several scales of roughness where many distinct scattering phenomena take place. These are particularly challenging to model and cannot be described consistently by geometric optics alone.

Recently, sophisticated BRDF models based on wave-optics were presented [YHW*18, WVJH17, HP17]. They are capable of modelling wave-optics phenomena and lead to a more realistic appearance. However, they are still limited to some approximations, e.g. ignoring multiple reflections, and, to the best of our knowledge, there is no sound validation with measured data for rough surfaces. Both limitations make it difficult to classify their agreement with reality which, in turn, hinders further improvement of the model.
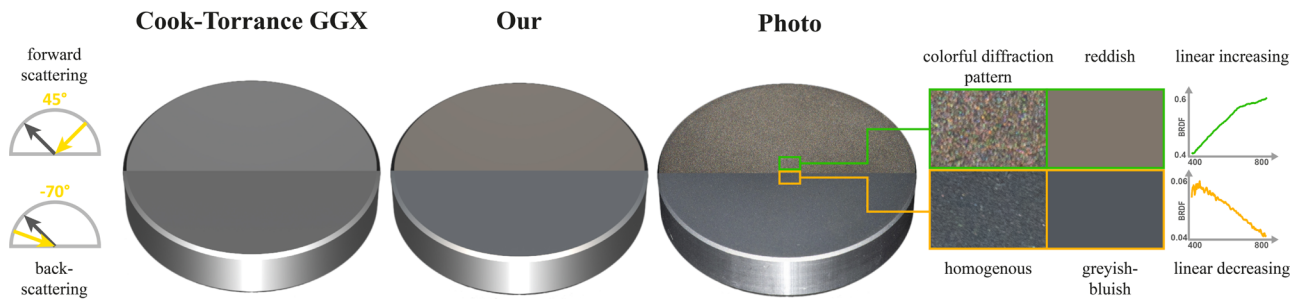
Figure 1: *The appearance of a rough aluminium sample (Sample 1) varies drastically when illuminated from different directions (cf. Photo). It changes from a reddish appearance in the forward scattering direction to greyish-bluish in the back-scattering direction. The BRDF spectra present an unusual linear shift towards long and short wavelengths. The speckle-like patterns indicate that this phenomenon originates from diffraction effects. The Cook–Torrance model cannot simulate such wave-optics phenomena (cf. Cook–Torrance GGX), whereas our BRDF model better approximates the observed diffraction phenomena at nearly no extra cost.*

Another disadvantage making them unsuitable for real-time applications is the high computational costs.

A deeper understanding of wave-optics phenomena is essential to overcome the limitations and further improve the simulation of light interaction with rough surfaces from visual and performance perspectives. Therefore, in this work, we experimentally investigate the interaction of light with rough surfaces and provide the following three contributions as summarised in Figure 1.

First, we acquired a multi-modal dataset of aluminium samples with varying roughness, where each sample is characterized in several ways: surface topography from a confocal microscope, measured spectral in-plane BRDF, macro photos under varying illumination angles and, finally, scattering simulations with a virtual goniometer. Such a rich dataset enables a deeper analysis of light interaction with rough surfaces and, consequently, allows us to validate or even improve existing models. Given the importance of such detailed datasets to the community, we make it freely accessible under the link https://cg.web.th-koeln.de/mmd/.

Second, we thoroughly analyse the acquired data and heuristically approximate the observed scattering phenomena. We found that diffraction takes place in all cases and dominates the appearance of the aluminium samples. We show that wavelength shifts lead to a reddish and bluish appearance, which can be related to forward and back-scattering. The wavelength shifts can be, surprisingly, described by a linear function. These observations are strengthened by the fact that data from all different measurement modalities and wave and geometric optics simulations corroborate our claims. We developed a simple heuristic model approximating such effects based on these new insights.

And third, we extend the Cook–Torrance model by a shift function to account for these diffraction phenomena. This BRDF model simulates diffraction effects without impacting the computational costs.

Our work is divided into seven sections. Section 2 discusses the related literature and presents an overview of analytical BRDF models based on geometric and wave-optics. Section 3 describes the experimental procedures. The description of light interaction with

aluminium samples and the analysis of the observations are given in Sections 4 and 5. We discuss the results and posit our theory in Section 5.7. In Section 6, our new BRDF model is introduced and conclusions are finally provided in Section 7.

2. Related Work

Measured BRDFs are paramount in analytically describing light interaction with real-world materials and validating reflectance models. Important databases and their limitations are presented in the following. Further, an overview of analytical BRDF models based on geometric and wave-optics is given.

2.1. Databases

The MERL database [MPBM03] provides densely sampled BRDFs of many materials and has been widely used to develop and validate reflectance models. The BRDFs are acquired with a camera that drastically shortens acquisition time but, on the flip side, only provides RGB values and introduces lens aberrations [Bur12]. The UTIA [FVH14, FV14] and the UBO2014 database [WGK14] provide BTFs of many textured materials, but both are also limited to RGB measurements. Furthermore, all scanned materials are inhomogeneous, making it challenging to analyse the light–matter interaction thoroughly.

Dupuy and Jakob [DJ18] recently introduced a spectral database where BRDFs are measured with a dynamic sampling strategy that significantly decreases measurement time. It is very beneficial for spectral BRDF validation. Nevertheless, additional information on the measured materials, such as surface topography, is necessary to analyse the light–matter interaction.

In the optics community, O'Donnell and Mendez [OM87] and Schröder *et al.* [SDC*11] acquired the surface topography and scattering of defined metal samples with varying roughness. Both measured the scattered data at three wavelengths; in both cases, one wavelength is outside the visible light spectrum.

None of the described databases provide dense spectral BRDF data and information about the surface topography at the same time. In this work, we created a dataset that combines many of these essential aspects to analyse the relation between light–matter interaction and surface roughness.

2.2. Geometric optics models

In computer graphics, light–matter interaction is commonly approximated with analytical BRDF models based on geometric optics, where light propagation is described in terms of rays. The underlying assumptions heavily simplify the computations, consequently allowing for the usage in real-time applications.

BRDF models can be divided into phenomenological, data-driven and physically based models [GGG*16]. In computer graphics, the latter has become most popular in the last two decades. These models use a few physically based and intuitive parameters to describe light interaction with different materials and surface types. They consider several scattering phenomena like multiple scattering, shadowing and masking, off-specular peak, and the Fresnel effect while, at the same time, obeying energy conservation, Helmholtz reciprocity and positivity. Moreover, physically based BRDF models provide an overall good trade-off between being artist-friendly and physically correct.

Microfacet-based models are a popular choice, particularly the Cook–Torrance BRDF model [CT81] combined with one of the available normal distribution functions [TR75, CT81, WMLT07, BSH12, Bur12, LKYU12]. Albeit their advantages, deviations can still be noted when comparing or fitting them against measured data. In particular, wavelength-dependent scattering phenomena are often not adequately represented by geometric optics approaches. This drawback has led to physically not plausible extensions that improve fitting results, e.g. using a specular albedo or two lobes [CT81, NDM05, Bur12, LKYU12].

Clausen *et al.* [CMF18] further showed that, for ColorChecker patches, there is a linear wavelength dependency in the forward and back-scattering at grazing incident angles. These wavelength shifts have been scarcely reported in the literature and are typical phenomena that geometric optics cannot explain. Consequently, they are not accounted for in the Cook–Torrance model.

2.3. Wave-optics models

One reasonable explanation for the deviations between model and measured data is diffraction, as stated by Holzschuch and Pacanowski [HP17]. Yan *et al.* [YHW*18] also noticed visual prominent diffraction phenomena on rough surfaces even when illuminated with partially coherent light.

Two historical approaches analytically describe light–matter interaction: the Rayleigh-Rice (RR) vector perturbation theory [Ric51, CJZ79] and the Beckmann–Kirchhoff (BK) scattering theory [BS87]. Both are complementary in their range of validity. The RR theory is valid for smooth surfaces for arbitrary incident and reflection angles. The BK theory is valid for rougher surfaces but only for small incident and reflection angles.

The Generalized Harvey Shack (GHS) theory [KHC11] combines the advantages of the previous approaches without their limitations. Nevertheless, Schröder *et al.* [SDC*11] noticed deviations between measured data and the GHS theory when dealing with rougher surfaces. The authors assume that these deviations result from measurement errors.

A few BRDF models were developed based on these theories. He *et al.* [HTSG91] extended the Cook–Torrance model using the BK scattering theory. Their model matches well the measured data of a few materials. Nevertheless, Ngan *et al.* [NDM05] showed that when fitting against the MERL database, He's model leads to similar results as the Cook–Torrance model.

Löw *et al.* [LKYU12] introduced a BRDF model based on the RR theory. Even though it is limited to smooth surfaces, it represents such cases from the MERL database very well. A different approach is presented by Dong *et al.* [DWMG16]. For the first time, the anisotropic appearance of metal samples was determined only by their micro-geometry. They demonstrate that both geometric- and Kirchoff-based approaches can model the appearance properly. However, a systematical validation of the proposed model with measured BRDFs is missing.

Holzschuch and Pacanowski [HP17] assume the surface reflectance as a superposition of the reflectance on the macro and micro-geometry. The first is characterized by the standard Cook Torrance model and the second by the modified Harvey Shack theory. The model can reproduce some wavelength-dependent phenomena observed in the MERL dataset but still carries the limitations of the modified Harvey Shack approach.

Yan *et al.* [YHW*18] derived a generalized BRDF representation where the three scalar diffraction theories, Harvey–Shack, GHS and Kirchhoff, can be alternatively used. Their model allows the simulation of full diffraction effects of arbitrary micron-scale heightfield geometries. The authors provide interesting renderings of a brushed metal patch with a clear reddish appearance in the forward scattering. Even though not discussed by the authors, this strongly reminds us of the wavelength shifts we analyse in this paper. The rendering results are only compared to photos; thus, a systematic validation of their renderings with measured data is missing.

3. Experimental Procedures

The scattering of light on rough surfaces is a complex and high-dimensional problem. The surface's roughness plays a decisive role in the interaction of light and, consequently, the material's appearance. To further investigate this relation, we generated aluminium samples with varying roughness, thus ruling out differences in material properties in our analysis. We used four measurement techniques to conduct a sound analysis: surface measurements, macro photos, spectral BRDF measurements and light scattering simulations. The aluminium samples and these methods are further described below.

3.1. Samples

We generated eight round aluminium samples since it is a cheap material and easy to process. Furthermore, it provides a high and

Table 1: *Sandblasting conditions to generate the eight aluminium samples with varying roughness.*

	Sample 1	Sample 2	Sample 3	Sample 4	Sample 5	Sample 6	Sample 7	Sample 8
Pressure (bar)	6.5	4	3	2	1	–	1	1
Distance (mm)	100	100	100	100	100	–	200	200
Abrasives (μm)	70-100	70-100	70-100	70-100	70-100	–	35	70–100
Roughness rms (μm)	2.39	1.76	1.20	0.98	0.52	0.10	0.66	0.43

almost uniform reflection over the light spectrum, and for an ideally smooth surface, the Fresnel equations describe well the light interaction. The necessary spectral refractive index and extinction coefficient of aluminium can be found in the literature [CSC*16].

We use the aluminium alloy AlMg3, which is more corrosion-resistant than pure aluminium [BGM*04]. While the reflectance of AlMg3 is slightly lower than that of pure aluminium, the spectral shape remains similar. We assume that these deviations are small compared to the investigated scattering phenomena and do not negatively influence our analysis.

All samples are 10 mm thick with a diameter of 50 mm and were first polished to a mirror-like finish. Then, all samples except one were sandblasted under varying conditions. For each sample, we modified the following conditions: pressure, distance and abrasives diameter, as specified in Table 1. As expected, increasing the pressure and decreasing the distance leads to a rougher surface. Note that using smaller beads as abrasives does not lead to a smoother surface, which can be attributed to the fact that the smaller beads are accelerated faster than the larger beads at the same pressure.

3.2. Surface measurements

As aforementioned, the surface finish impacts the scattering of light and, thus, the material's appearance. It is of great importance when dealing with wave-optics phenomena. Therefore, the surface topographies of all samples were measured with a white light confocal microscope (Nanofocus μsurf Generation C) that provides, in combination with the 320S lens, a lateral and vertical resolution of 625 and 20–40 nm, respectively. A single shot captures an area of 320×320 μm. A stitching mode can measure more extensive areas, allowing scanning areas up to 7.3 mm^2.

In Figure 2, the surface topographies of the eight aluminium samples are shown. For each one, an area of 1280×1280 μm was scanned with a vertical resolution of 20 nm for Samples 5, 6 and 8, and of 40 nm for the remaining. The variation in resolution is due to the device's limitations when scanning rougher surfaces.

The figure illustrates that the sandblasted samples' topographies consist of randomly distributed spherical holes. Except for Sample 8, where the base surface is still visible, all others show an isotropic random surface. Sample 6 was not sandblasted but still contains visible scratches, influencing the scattering behaviour [WVJH17].

3.3. Macro photos

We acquired macro photos under a fixed camera position and varying illumination angles to obtain spatial information on the light
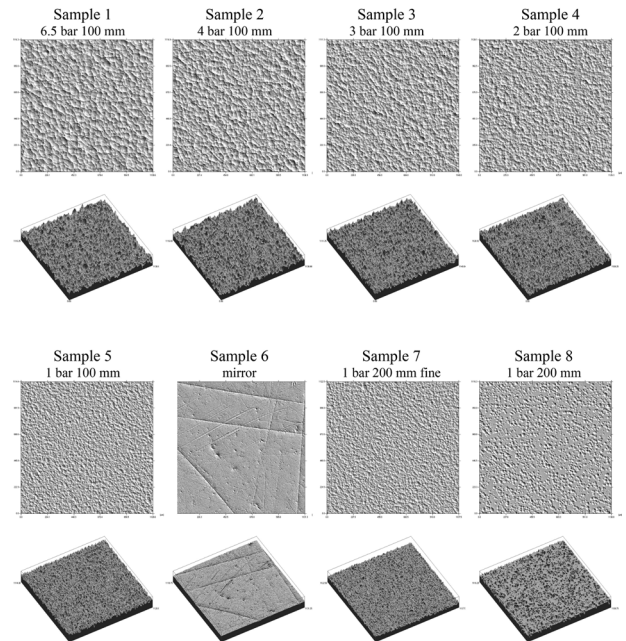

Figure 2: *Top and 3D views of the samples' surface topographies measured with a confocal microscope. Except for Sample 6, the surfaces consist of randomly distributed holes caused by the glass beads of the sandblaster.*

interaction with the aluminium samples. A simple goniometer was used consisting of a collimated high power LED, which can be moved on a semi-circle around the sample, and a Nikon D810 with a micro Nikkor 105 mm lens mounted on a tripod at 45° in regards to the sample surface. The camera is calibrated by performing a manual white balance with a Spectralon sample illuminated with the LED light source. The macro photos are captured with illumination angles varying from −70° to 70° in 5° steps.

3.4. BRDF measurements

The macro photos provide spatial information, but the spectral domain is limited to RGB values. Since wave-optics phenomena are strongly wavelength-dependent, spectral BRDFs are necessary. We measured the in-plane BRDF of all samples with a custom-built gonioreflectometer consisting of a fixed collimated halogen light source and two goniostages, one to rotate the sample and the other to rotate the detector. A glass fibre cable connects the detector to a scientific-grade spectrometer (Ocean Optics QE Pro) with high sensitivity in the wavelength range of 250–1050 nm. The measurement
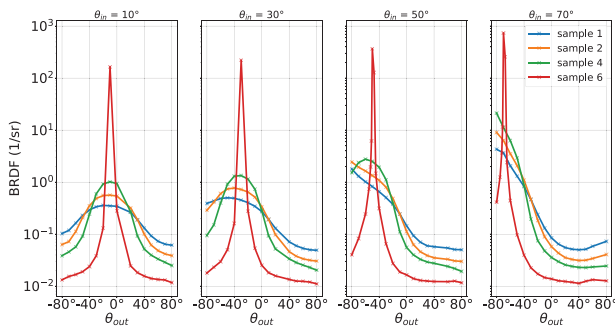
Figure 3: *Reflectance distribution of Samples 1, 2, 4 and 6 at wavelength 600 nm. Sample 6 with a mirror finish has a narrow specular peak. Instead, the rougher samples scatter more broadly and present an off-specular peak for large incident angles.*

spot has a diameter of around 2.5 mm when measuring normal to the sample. At measurement angles deviating from the normal direction, the measurement spot is horizontally enlarged by one over the cosine of the measurement angle. The maximum measurement angle is 85°, and consequently, the maximum measurement spot has a horizontal diameter of approximately 30 mm. In the back-scattering direction, the detector blocks the light source in the range of ±5°. The device is calibrated with a relative calibration method using Spectralon and the associated reference BRDF provided by Durell *et al.* [DSM*15]. We acquired the in-plane BRDF of all samples with a sampling resolution of 10° in the incident domain (θ_{in}) and dynamic resolution in the reflection domain (θ_{out}). We discarded Sample 7 due to its inhomogeneous surface.

3.5. Scattering simulations

Another essential piece of information is the scattering paths, which is particularly important when dealing with rough surfaces where multiple scattering occurs. We developed a virtual gonioreflectometer to simulate light interaction with the topographies from the aluminium samples, assuming that each facet is a perfect mirror. We ran simulations to gather information on the energy coming from rays that reach the sensor after a different number of reflections, taking Fresnel into account. Even though the simulation only considers geometric optics, it provides valuable insight into the trends between first and multiple reflections for forward and back-scattering.

4. Observations

This section describes the observed light interaction with the rough aluminium surfaces. The overall scatter characteristics of all samples are compared, the visual appearance is evaluated based on the macro photos, and the angle and wavelength dependency is investigated using the in-plane BRDF.

4.1. Scatter characteristic

As intended, the aluminium samples scatter light differently. Figure 3 shows the reflectance distributions at 600 nm of Samples 1, 2, 4 and 6 for various incident angles. The BRDF of the smoothest

sample (Sample 6) has a clear peak in the specular reflection and falls quickly to almost zero, resulting in a narrow specular lobe with a high dynamic range of five decades. In contrast, the roughest sample (Sample 1) scatters light in a wide range of angles, and the off-specular reflection for large incident angles, as reported by Torrance and Sparrow [TS67], can be observed. Both samples have back-scattering at grazing incident angles, which is stronger at the rough sample. The reflectance distributions of the remaining samples are within these two extremes.

4.2. Visual appearance

As described in Section 3.3, the macro photos help to get a first impression of light scattering on rough surfaces. Different from spectral measurements, they provide spatial resolution, which is important for analysing spatially varying phenomena, such as diffraction.

Figure 4 provides a macro photo of forward scattering for each sample, with a detailed view and the average colour of the insets. Except for Sample 6, a colourful scattering pattern can be observed, leading to an average reddish appearance.

This colour pattern resembles speckle patterns typically observed when rough surfaces are illuminated with coherent light, e.g. laser. The speckle effect results from the interference of many waves with varying phases and amplitudes but with the same frequency. A similar effect can also be observed when illuminating with partially coherent light [YHW*18, SY21], e.g. natural light. We conclude that these patterns, as well as the average reddish appearance, originate from diffraction on the surface.

In the following, we focus on evaluating the measurement results of the roughest sample (Sample 1). In this case, the diffraction phenomena are more prominent, as shown in Figure 4, and the low dynamic range simplifies the light scattering analysis.

Figure 1 shows macro photos of Sample 1 under two different illumination angles, highlighting the differences between forward and back-scattering. Note that the exposure time is adapted to achieve the same brightness for both cases. It is clear that the visual appearance of the rough aluminium sample strongly depends on the illumination angle. While the sample appears greyish-bluish for back-scattering, a colourful pattern occurs for forward scattering, leading to an, on average, reddish appearance. Except for the mirror-like sample, all others present similar behaviour.

The BRDF spectra, on the right side of Figure 1, indicate that the different colours originate from a close to linear increase or decrease of the reflectance spectrum. The similar linear behaviour in both reflectance cases leads us to suspect that diffraction not only takes place in the forward scattering but also in the back-scattering.

4.3. Angle and wavelength dependency

To further understand the observed diffraction phenomena and to analyse their angle and wavelength dependency, the acquired in-plane BRDF of Sample 1 is examined. Since the analysis of the in-plane BRDF with almost 300 spectra is complicated, we introduced a simplified RGB representation as illustrated in Figure 5. On the *x*- and the *y*-axis, the reflection (θ_{out}) and incident angles
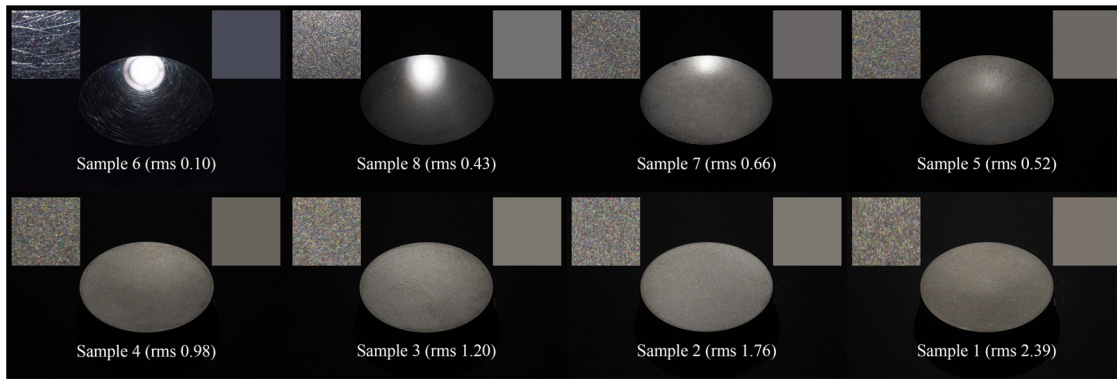
Figure 4: *Eight aluminium samples with surfaces varying from smooth (top-left) to rough (bottom-right). For each sample, we show a macro image in the centre, a detailed view on the left, and the average colour of the detailed view on the right. Colourful diffraction phenomena can be observed for all samples and an, on average, reddish appearance. This colour shift is particularly strong for rough surfaces where the appearance strongly deviates from the expected greyish of aluminium.*
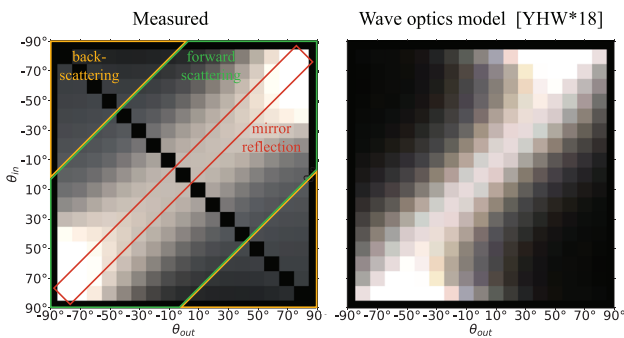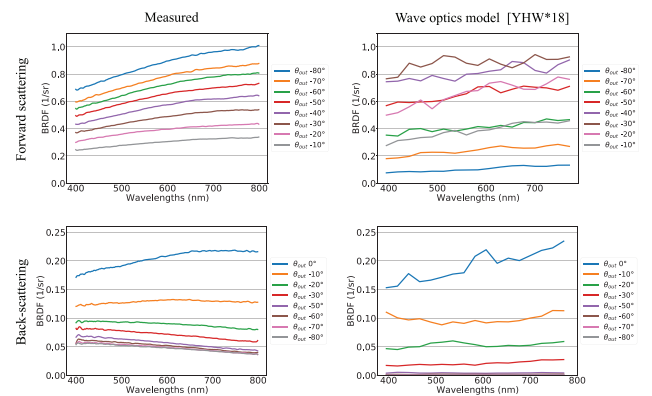

Figure 5: *Measured in-plane BRDF of Sample 1 (left) and simulated BRDF (right) using the wave-optics model from Yan* et al. *[YHW*18]. The reddish tone in the mirror reflection (centre of the forward scattering) changes continuously into a greyish-bluish tone in the back-scattering region. For the simulated data, the back-scattering effect is not contemplated.*

Figure 6: *On the left side, the measured spectral BRDFs of Sample 1 for forward and back-scattering at $\theta_{in} = 40°$. On the right, the same for simulated scattering using the wave-optics approach from Yan* et al. *[YHW*18]. The measured BRDF spectra are linearly shifted towards long and short wavelengths in the forward and back-scattering. Even though the increasing trend is noticeable in the simulations, back-scattering is not contemplated.*

(θ_{in}) are plotted, and each square represents an individual measurement of the in-plane BRDF. To generate such an RGB image, we virtually illuminated the spectra by multiplying them with the standard illuminant D65 spectrum and the incident angle's cosine. The resulting spectra are converted into the BT709 colourspace. Hence, a uniform BRDF spectrum results in an RGB value of (1,1,1) perceived as white when adapted to D65.

In agreement with our previous observations, Figure 5 (left) shows that the measured BRDF of Sample 1 appears reddish in the forward scattering and greyish-bluish in the back-scattering. A new interesting insight is a continuous transition between the reddish and greyish-bluish appearance in forward and back-scattering.

The spectral data provide further information, as shown on the left side of Figure 6. For an incident angle of 40° we observe close to linear increasing and decreasing spectra for forward and back-scattering, respectively. The spectra within these two extremes are tilted continuously from a positive to a negative slope.in

When comparing with the Fresnel reflectance spectra of aluminium, we note that the general behaviour is present but without the tilt. However, it is the only physically plausible wavelength-dependent term in BRDF models based on geometric optics. Hence, it is clear that these approaches cannot model the observed colour pattern in the forward scattering and the linear shift tendency.

5. Analysis

In the previous section, we introduced three assumptions related to the observed wavelength shifts on rough aluminium samples. First, the wavelength shifts are caused by diffraction; second, they have a linear behaviour; third, they are shifted towards long and short wavelengths in the forward and back-scattering, respectively.

These observations are new to the computer graphics and optics community. To the best of our knowledge, only the works by Levesque *et al.* [MPL16, LD18] and Clausen *et al.* [CMF18, CMFW19] report these phenomena. Still, none provides a sound investigation or explanation. In the following, we present a thorough analysis of the observed wavelength shifts, providing a better understanding that supports our assumptions and serves as the basis for new and simpler BRDF models.

5.1. Diffraction phenomena

To confirm that the observed scattering phenomena are indeed caused by diffraction, we used the BRDF model provided by Yan *et al.* [YHW*18] to simulate wave-optics scattering of Sample 1. As mentioned in Section 2, this model has the advantage of integrating the GHS theory and, consequently, being valid for all angles and rough surfaces. In addition, it works directly on the measured micro-geometries.

The micro-geometry was first sampled in 1 μm steps, and then the in-plane BRDF was simulated by evaluating an area of 500×500 μm for 20 different wavelengths.

Figure 5 (right) shows the RGB representation of the simulated in-plane BRDF. In the mirror direction, a reddish colour can be observed, similar to the one in the measured data (left). As illustrated on the right side of Figure 6, the corresponding simulated spectra have the same increasing trend as the measured data on the left side. The matching reddish colour and the increasing trend indicate that the observed wavelength shift in forward scattering is caused by diffraction.

The simulation, however, does not account for the decreasing trend in back-scattering as observed in the measured data. One reasonable explanation is that multiple reflections are not considered in the simulation. Apart from this, there are other noticeable differences between measured and simulated data.

First, the simulated BRDF has a stronger specular reflection than the measured BRDF, which is illustrated in Figure 5 by the narrow forward scattering and the near lack of back-scattering. Again, the ignored multiple reflections are a reasonable explanation.

Second, the simulated BRDF has weaker off-specular peaks than the measured BRDF. Even more, for grazing incident angles, the off-specular peak shift of the simulated data is towards smaller reflection angles, contradicting the measured data. We noticed similar behaviour with the scatter simulation using the virtual goniometer. A plausible explanation for this deviation are discretization issues regarding the micro-geometry. However, the analysis of this issue is beyond the scope of this work and is left as future work.

5.2. Linear wavelength shifts

When dealing with scattering models, a wavelength dependency of $\frac{1}{\lambda^4}$ is often mentioned. A linear wavelength dependency, as observed in Section 4.3, is very unusual, which was one of the primary motivations for this research.
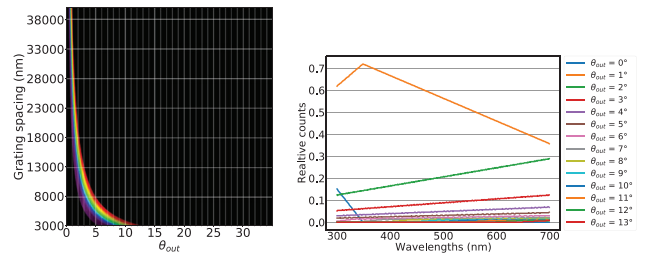
(a) Light diffraction at gratings. (b) Corresponding spectra.

Figure 7: *First order of light diffraction at gratings with varying spacing (a) and the resulting spectra when binning over the diffraction angles (b). Diffraction is a reasonable explanation for the linear wavelength shifts observed on rough surfaces.*

The sandblasted aluminium samples have a stochastically created surface with an almost Gaussian height distribution. The superposition of many phase gratings with varying orientations, periods, amplitudes and phases can approximate this kind of surface [SDC*11]. To investigate the observed linear wavelength dependency, we further simplified this approach by approximating the rough surfaces by the superposition of many amplitude gratings with different spacing. For each grating, the relationship between the grating spacing, incident angle and the angle of the diffracted light is described by the diffraction equation:

$$\theta_{out} = \arcsin(\sin(\theta_{in}) - \frac{m\lambda}{d}), \qquad (1)$$

where the parameters m and d are the diffraction order and grating spacing, respectively. In Figure 7a, the first order of light diffraction at gratings with varying spacing is plotted. The plot comprises two interesting characteristics. First, when the grating spacing decreases, the light is more strongly diffracted. Second, small wavelengths are diffracted weaker than long wavelengths.

The detector of a gonioreflectometer or the human eye has a limited angular resolution, thus integrating over an angle range. When simulating this integration by binning the grating diffraction with a bin size of $1°$, the resulting spectra are shown in Figure 7b. All spectra have a clear linear dependency, where at diffraction angles of $0°$ and $1°$, the slope is negative and at the remaining angles positive. The negative slope results from the fact that there are practically no long wavelengths in the first two bins.

These results show that the linear dependency does not originate directly from diffraction on the surface. But instead from the integration of diffraction over an angle range. Even though our approach is still a rough approximation, it offers a reasonable explanation for the observed linear dependency in the measured data.

5.3. Local fit of linear shifts

As stated in Section 4.3, the measured spectra seem to be tilted versions of the Fresnel reflectance spectra. To verify this assumption, we heuristically describe the observed wavelength dependency by the multiplication of the Fresnel term with a linear function:

$$f_{norm}(i, \lambda) = (m\lambda + b) \cdot F^p(i, \lambda), \qquad (2)$$
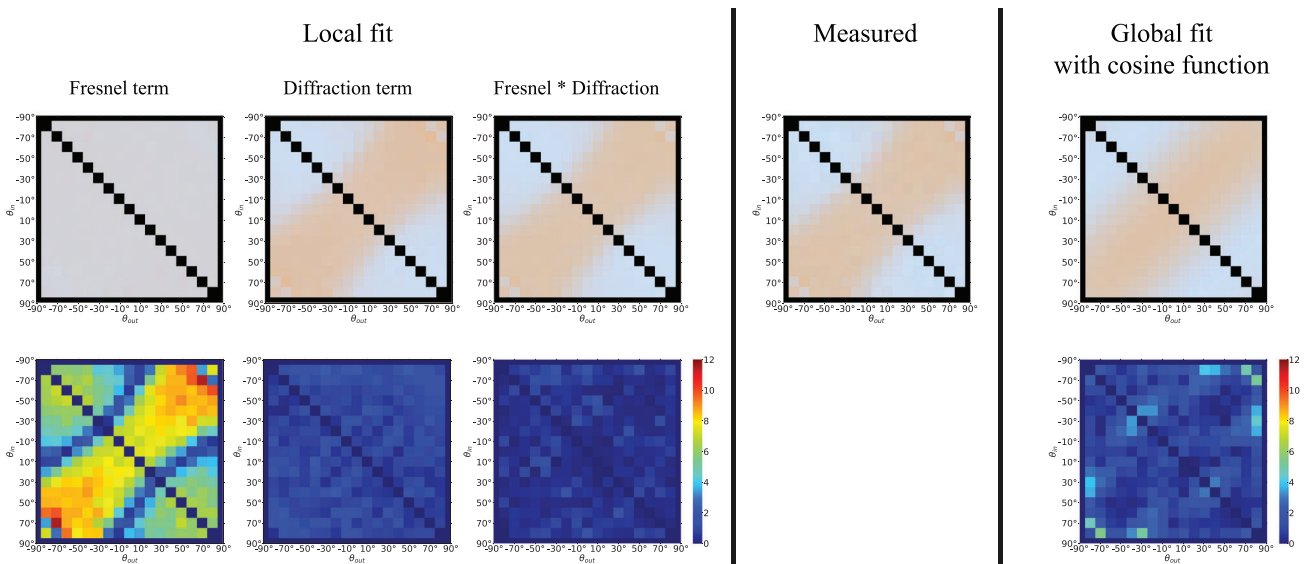
Figure 8: *Comparison of the local and global fit with the measured data for Sample 1 using the RGB representation. On the left, the local fit is divided into the Fresnel and diffraction term. The Delta E's 2000 between the fitted and the measured BRDFs are shown on the bottom row. In the case of local fit, the Delta E's remain below the perception threshold. The global fit leads to slightly higher Delta E's but can still adequately reproduce the measured data.*

where m and b are, respectively, the slope and y-axis intersection of the linear function, and the exponent p takes into account the effect of multiple reflections.

We fit this model against the measured in-plane BRDF of Sample 1. The parameters m, b and p are determined for each reflectance spectrum separately, and we refer to this approach as local fit. Before conducting the local fit, the BRDF spectra are normalized on an arbitrary wavelength λ_n, in our case 600 nm, to obtain the spectral characteristic and remove any global scaling factor. The Fresnel spectrum is likewise normalized, and b is chosen to rotate the spectrum around λ_n by the linear function. This heuristic model fits the BRDF spectra very well with an r2 score > 0.95 and > 0.90 for, respectively, 88% and 93% of all BRDF spectra.

In Figure 8, the fitting results are further investigated from a perceptual perspective. As expected, the Fresnel term has a neutral greyish appearance for almost all incident and reflection angles, while the colour variation comes entirely from the diffraction term. Again, it is evident that the Fresnel term cannot model the colour modulation properly, leading naturally to large Delta E 2000 (dE00) values up to 12. Nevertheless, the Fresnel term still plays an important role, which can be observed by lower dE00 values when accounting for it, as in Equation (2). In rare cases, barely perceptible differences with dE00 values above the just noticeable difference of 1 occur.

Both the r2 score and the dE00 values confirm our assumption that the observed diffraction phenomenon has a linear wavelength-dependency, in agreement with the observations made by Levesque *et al.* [LD18]. This result is of substantial value for developing a simple BRDF model that considers these phenomena.

5.4. Global fit of linear shifts

Albeit the successful fitting by a linear function combined with the Fresnel term, each spectrum was still considered independently. However, a global model is necessary to describe the diffraction phenomena in an analytical BRDF model.

Similarly to the local model, we can describe the global model as

$$f_{norm}(i, o, \lambda) = shift(i, o, \lambda) \cdot F^p(i, \lambda). \qquad (3)$$

$$shift(i, o, \lambda) = m(i, o) \cdot \lambda + b. \qquad (4)$$

This model differs from Equation (2) only by the dependency of the slope distribution m on the incident and reflection direction. We found that a cosine function parametrized by θ_m describes this distribution well:

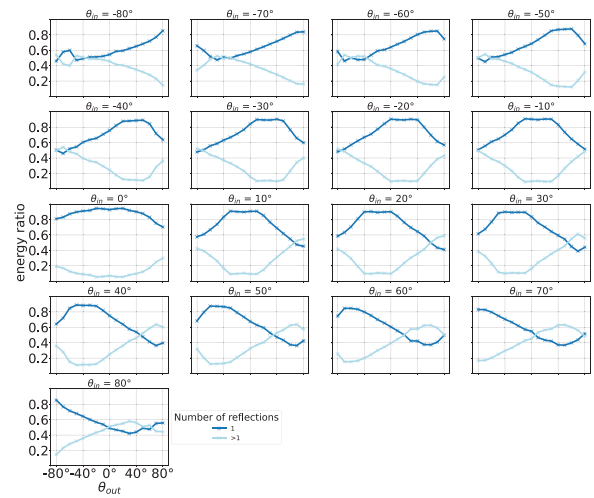$$m_{cosine}(i, o) = h \cdot cos(w \cdot \theta_m) + t_y, \qquad (5)$$

where w and h scale the cosine function in the x- and y-axis, and t_y translates the function along the y-axis. Note that θ_m is the angle between the macrosurface normal n and the microsurface normal m.

Figure 9 provides an example of a global fit for the slope distributions of Sample 1. For each incident angle, we plot in blue the local fits and in orange the global fit using the cosine function. The figure contains two interesting characteristics. First, the slope values are symmetrical around the mirror reflection, and second, they are periodic. The latter is even more noticeable for smoother samples. We also note that the cosine function fit is adequate, only having
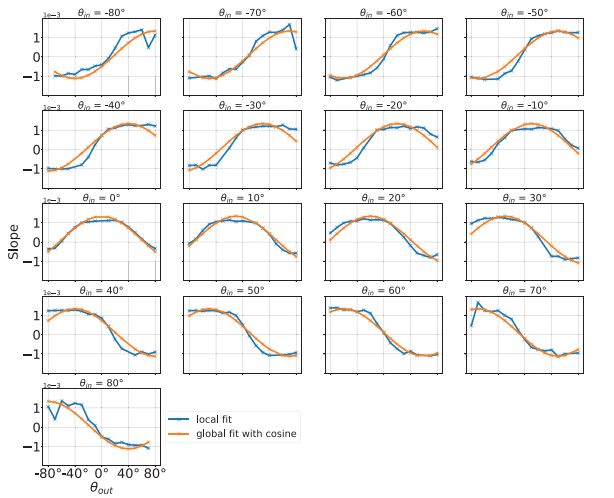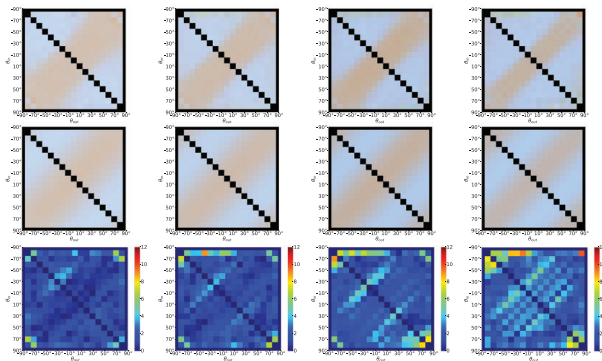
Figure 9: *Slope distribution (y-axis) of Sample 1 resulting from the local fit (blue line) and the global fit using a cosine function (orange line).*

Figure 10: *Results of our global fitting model for Samples 2–5.*

issues with the fast transition from a positive to a negative slope. Similar fitting results are achieved for the other samples.

Figure 8 shows on the right side the global fitting result for Sample 1, while Figure 10 further shows results for Samples 2–5. Overall, the model provides a good fit with increased precision for rougher surfaces. For smoother surfaces, the colour differences increase, leading to noticeable differences for Sample 5.

A reasoned explanation for this trend is the inadequacy of the cosine function to model fast transitions, which are sharper on smoother surfaces. Furthermore, for smooth samples, the signal-to-noise ratio is very low for reflection angles away from the specular reflection, which complicates the fitting process. This problem occurs especially in the mirror-like sample, which our model cannot fit properly.

Figure 11: *Simulation results show in blue the percentage of energy coming from single reflection rays and in light blue multi-reflection rays for wavelength 380 nm and varying incident angles.*

5.5. Scatter decomposition

Previously, we focused on analysing light scattering without having information about its composition. It is helpful to decompose the light scattering into the number of reflections to better understand the observed scattering phenomena, mainly the different diffraction phenomena in the forward and back-scattering. The decomposition can be achieved using our virtual goniometer (Section 3.5) combined with the micro-geometries acquired with the confocal microscope. Figure 11 shows the decomposition of the light scattering of Sample 1 into the first (blue) and multiple reflections (light blue) for different incident angles. When further decomposing the multi-reflections, we noted that the trend is the same for each number of reflections, so there is no significant difference between two or more reflections in terms of behaviour.

The plot demonstrates that, as expected, first reflections dominate the forward scattering for all incident angles. Away from the forward scattering, the percentage of multiple reflections increases and, for large incident angles, multiple reflections dominate the back-scattering. There is a correlation between the distribution of the first reflection and the slope distributions in Figure 9 confirming our assumption that the wavelength shifts toward long and short wavelengths are related to first reflections in forward scattering and multiple reflections in back-scattering. Furthermore, the scattering simulations explain the plateau observed in the slope distributions, i.e. it is present when first reflections account for nearly 100% of the captured rays.

The strong influence of multiple reflections in the back-scattering direction also explains why the wave-optics simulation (Section 5.1) failed to capture such effects since it does not account for them.

5.6. Diffraction on dielectric surfaces

The observed wavelength shifts were also observed for dielectric materials, e.g. Spectralon SRS-99 [LD18, CMFW19],

ColorChecker patches and grey wall-paint [CMF18]. This phenomenon is less prominent for dielectrics since internal diffuse scattering often dominates the overall reflectance at small angles. Nevertheless, surface scattering increases at grazing angles due to the Fresnel effect, and the shift becomes perceivable.

Similar to the aluminium samples, we prepared samples of the Spectralon SRS-02 with different roughness levels. We sanded each sample with sandpaper of varying grain sizes, from 60 to 5000 on the CAMI scale, where lower numbers indicate rougher samples. Then, we measured the in-plane BRDF and retrieved the slope of the spectra with the local fit approach. We assume that SRS-02 reflects light uniformly, so we do not consider the Fresnel effect, which is equivalent to setting $p = 0$ in Equation (2).

Spectralon SRS-02 has a 2% reflectance and scatters light in an almost ideal diffuse manner. Similar to the more well-known Spectralon SRS-99, it has no wavelength preferences. The strong light absorbance eliminates internal diffuse scattering and, thus, allows for the analysis of surface scattering.

When analysing the wavelength shifts of this material, we note some interesting characteristics in line with our previous observations. Figure 12 shows the slope distributions for three different roughness (60, 1000, 2500). For roughness 60, back-scattering dominates. At an incident angle $0°$, the slopes are distributed as a valley with a maximal negative slope around the incident angle. When the incident angle increases, the valley accompanies the back-scattering direction while the slope for the forward scattering increases. For roughness 2500, we observe a reverse behaviour, which leads us to assume that the forward scattering dominates the back-scattering in this case. Contrary to the previous two roughness, for roughness 1000, the wavelength shifts caused by forward and back-scattering compensate each other, leading to a uniform slope distribution at incident angle $0°$.

These results demonstrate that the wavelength shifts take place not only on conductive but also on dielectric surfaces, which again confirms the diffraction hypothesis. Furthermore, it confirms our assumption that forward and back-scattering lead to shifts towards long and short wavelengths.

5.7. Discussion

From the spectral BRDFs, we observed wavelength shifts in the responses, which are not caused by measurement errors, as proven by Clausen *et al.* [CMFW19]. The varied analysis with the acquired multi-modal dataset points towards a diffraction-based effect. We note that the shifts are linear when compensating for the Fresnel effect, an unusual optics behaviour. Our local and global fitting models confirm this linear tendency, and the grating simulations point towards phenomena related to the integration of diffraction effects. We suspected a further dependency on the number of reflections, which the scattering simulations confirmed. Finally, we showed that these are not phenomena particular to conductors by performing the same analysis with a dielectric material.

Based on the presented experimental analysis of light interaction with rough surfaces, we posit the following theory:
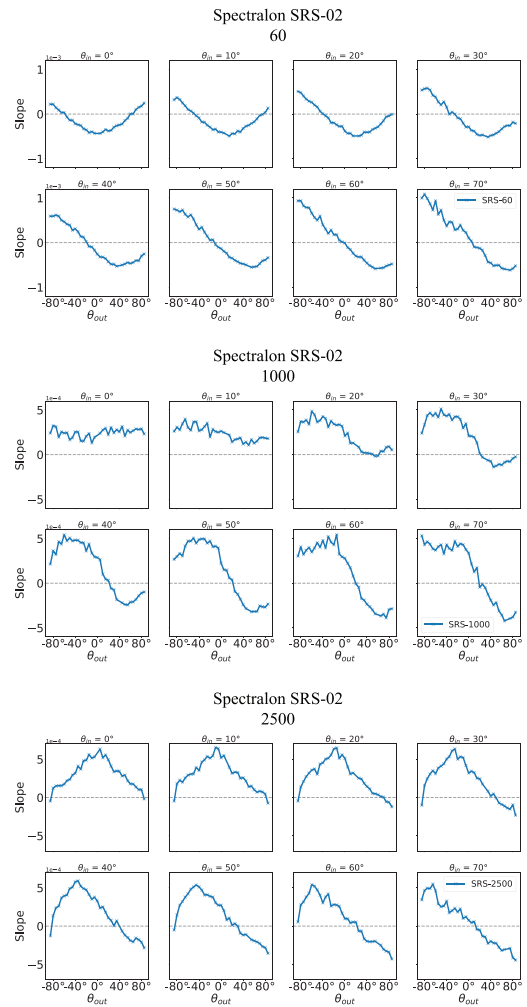
Figure 12: *Slope distributions locally fitted with a linear function of Spectralon SRS 02 sanded with grain size in the CAMI scale of 60, 1000, 2500. Back-scattering dominates for roughness 60, while forward scattering dominates for roughness 2500. For roughness 1000, forward and back-scattering compensate each other.*

Diffraction occurs on rough surfaces, dielectric and conductive, leading to an on average reddish and bluish appearance in forward and back-scattering, respectively. These diffraction phenomena are linearly wavelength-dependent; thus, a linear function describes them well. The shift towards long wavelengths originates from light scattered a single time. Conversely, the shift towards short wavelengths originates from multiple reflections. These phenomena dictate the overall visual appearance of rough conductors with a neutral reflectance. On the other hand, at rough dielectrics, they are only prominent at grazing angles.

We showed that the colour shift is, at least for the investigated aluminium samples, adequately fitted by the simple analytic model presented in Equation (3). The presented shift function can be used to extend microfacet BRDF models, like the classical Cook-Torrance

model. As shown in the following section, this is a straightforward and computationally cheap approach to simulate diffraction.

Moreover, the presented model still has limitations as it is only valid for a limited range of surface types. Our model struggles to fit the slope distribution of roughness 1000, where the forward and back-scattering compensate for small incident angles but become more prominent with increasing angles. A more general approach could come from the superposition of two weighted functions separating the diffraction phenomena caused by first and multiple reflections. The weights could be defined by the ratio of first and multiple reflections.

6. Application

So far, we analytically described in Equation (3) the observed wavelength shifts on rough surfaces caused by diffraction. This section shows how microfacet models based on geometric optics can be easily extended by the shift function (Equation 4). Further, we demonstrate that the new diffraction model improves the fitting of measured BRDFs of conductors and dielectrics in all cases. Finally, we compare renderings computed with the Cook–Torrance and our diffraction model.

6.1. BRDF model

The Cook–Torrance model in Equation (6) describes the light reflection from rough surfaces. The model approximates the material microsurface with statistically distributed tiny flat mirrors. The distribution of the mirrors is defined by the normal distribution function D, the reflection by the Fresnel equations, and the shadowing and masking by the geometric term G. A detailed explanation of the Cook–Torrance model is given by Walter *et al.* [WMLT07].

$$f_r(i, o, n, \lambda) = \frac{F(i, h_r, \lambda)G(i, o, h_r)D(h_r)}{4|i \cdot n||o \cdot n|} \quad (6)$$

The Cook–Torrance model is a popular BRDF model because it is physically based, intuitive and straightforward. Further, it is proven that the model approximates well the light reflection of different material and roughness types [NDM05, WMLT07, CMF18]. However, wave-optics phenomena are not considered, leading to clear perceivable deviations from reality, particularly for rough conductors. Therefore, we extended the Cook–Torrance model with the observed wavelength shifts by multiplying the model with the shift function described in Equation (4).

$$f_{diff}(i, o, n, \lambda) = shift \cdot f_r \quad (7)$$

Our model assumes that the overall scattering is well described by the Cook–Torrance model, consequently, by geometric optics and that the shift function approximates the observed diffraction phenomena. This model describes the first reflection on the material surface. Multiple reflection and internal scattering are not considered. Nevertheless, both phenomena are significant for dielectrics and can be approximated by adding an ideal diffuse albedo.

$$f_{dielectric}(i, o, n, \lambda) = \frac{r_d}{\pi} + f_{diff} \quad (8)$$

We observed that for both the conductive and dielectric version of our BRDF model, the exponent p and the offset parameter t_y of the global model (Equation 3) have a marginal influence on the fitting of the measured BRDF. Hence, we did not include them in the BRDF model.

6.2. Fitting

To validate our diffraction model, we fit the Cook–Torrance and our model against the measured in-plane BRDFs of the aluminium samples (conductors) presented in this paper and the 24 ColorChecker patches (dielectrics) provided by Clausen *et al.* [CMF18].

The GGX distribution and geometric function defined by Walter *et al.* [WMLT07] are used for all models. The fitting process and the implementation of the Fresnel equations are different for conductors and dielectrics, as explained in the following.

6.2.1. *Aluminium samples*

To fit the in-plane BRDFs of the aluminium samples, we use the Fresnel implementation of Mitsuba 2 [NDVZJ19], which provides a modified implementation of the equations given by Möller [Möl88]. The Fresnel equation is parameterized by the complex refractive index of aluminium. Consequently, for the Cook–Torrance model, only the roughness parameter α and for our model, additionally, the parameters w and h of the shift function have to be determined.

The fitting of the parameters is performed with the non-linear least squares minimization function of the library *lmfit* [lmf]. The Levenberg–Marquardt fitting method and the cost function by Löw *et al.* [LKYU12] are used. Figure 13a illustrates the fitting result of Sample 1. In the top row, the fitted in-plane BRDF with the Cook–Torrance model (left) and our model (right), as well as the measured in-plane BRDF (centre), are shown. The dE00 between the respective fitted and measured BRDF is depicted in the bottom row. The figure demonstrates that the scatter distribution of the Cook–Torrance and our model is the same, but the colour appearance is different. Our model better fits the yellowish and bluish appearance of the measured BRDF in the forward and back-scattering. It outperforms the Cook–Torrance model at all measurement points as confirmed by the dE00 plots and the, on average, lower dE00 by two. Similar fitting results can be observed at all sandblasted aluminium samples as shown in Table 2. The fitting improvements diminish with decreasing roughness, which can be explained by the diminishing influence of the wavelength shifts on smooth surfaces.

Although our model improves the fitting of the measured BRDFs, there are still differences. Our model struggles to fit the scattering distribution while fitting the colour appearance well.

(a) Aluminum Sample 1.

(b) ColorChecker Patch 4.
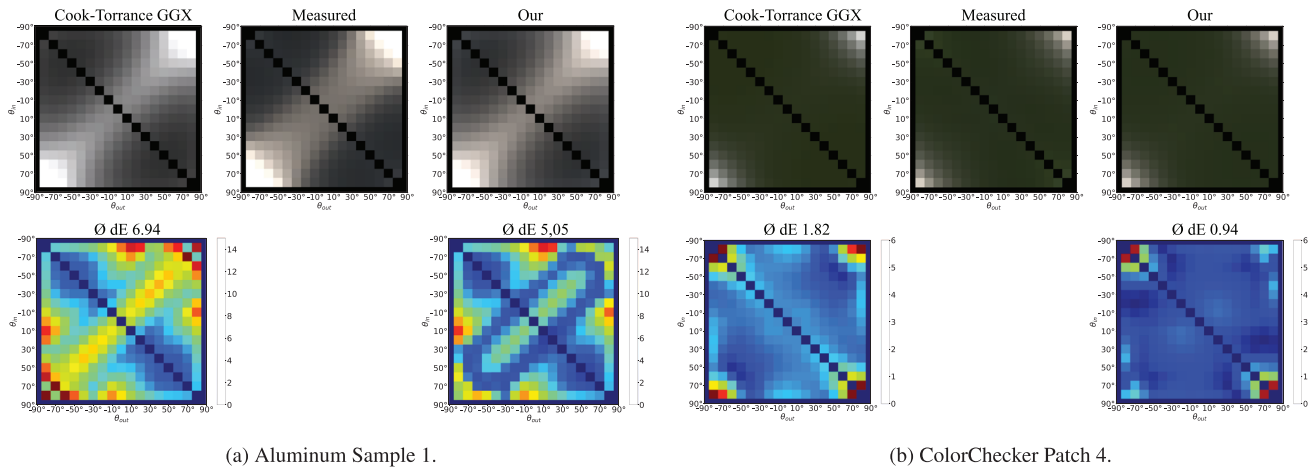
Figure 13: *Comparison of the fitting of a conductor (a) and a dielectric (b) with the Cook–Torrance and our model.*

Table 2: *Averaged dE 2000 between the measured in-plane BRDFs of the aluminium samples (top table) and ColorChecker patches (bottom table) and their respective fittings with the Cook–Torrance and our model. For all samples, our model outperforms the Cook–Torrance model.*

Aluminium	Sample 1	Sample 2	Sample 3	Sample 4	Sample 5	Sample 6
Cook–Torrance GGX	6.94	7.11	7.74	9.23	6.97	17.48
Our	5.02	5.83	6.32	7.46	6.02	17.05
ColorChecker	Patch 1	Patch 4	Patch 10	Patch 14	Patch 22	Patch 24
Cook–Torrance GGX	1.69	1.82	1.47	1.23	1.66	2.37
Our	0.95	0.94	1.09	0.81	1.27	0.92

We assume that the samples' microsurfaces consisting of randomly distributed cavities, are not well represented by microfacet models, which approximate the microsurface by tiny flat mirrors. It is well known that not only the microfacet normals' distribution but also their arrangement considerable influence the scatter distribution.

For Sample 6 (mirror sample), we observed another fitting issue. The measured BRDF values at grazing incident angles were much smaller than the simulated ones. We suspect that our gonioreflectometer fails to measure the BRDF of smooth surfaces under grazing angles, but more investigation is necessary. In any case, for this sample, measurements under grazing incident angles are weighted less in the fitting process.

6.2.2. ColorChecker patches

The ColorChecker patches' fitting differs from the aluminium samples' fitting due to the unknown refractive index and the diffuse albedo. Both have to be determined additionally to the fitting parameters of conductors.

We use the convenient approximation of the Fresnel equation for dielectrics introduced by Cook and Torrance [CT81]. The Fresnel equation is further simplified by assuming that dielectrics' refractive index (η) is wavelength independent.

The fitting process is divided into a non-linear and a linear optimization process, where the latter is a sub-process of the non-linear optimization process. The model parameters α, η, w and h are determined in the non-linear optimization, where w and h are only determined for our diffraction model. For the linear optimization, linear regression is employed to determine the wavelength-dependent diffuse albedo r_d.

The fitting result of the ColorChecker Patch 4 in Figure 13b demonstrates that our model outperforms the Cook–Torrance model also when fitting dielectrics. Our model improves the fitting of the specular reflection, particularly visible at grazing angles and the fitting of the diffuse reflection. The Cook–Torrance model tries to compensate for the lack of the wavelength shift in the specular reflection with the diffuse albedo, which leads to a reddish-tinted diffuse albedo. The dE00 plots confirm this observation; the dE00 is not only lower at grazing angles but also at small angles, where the diffuse reflection dominates.
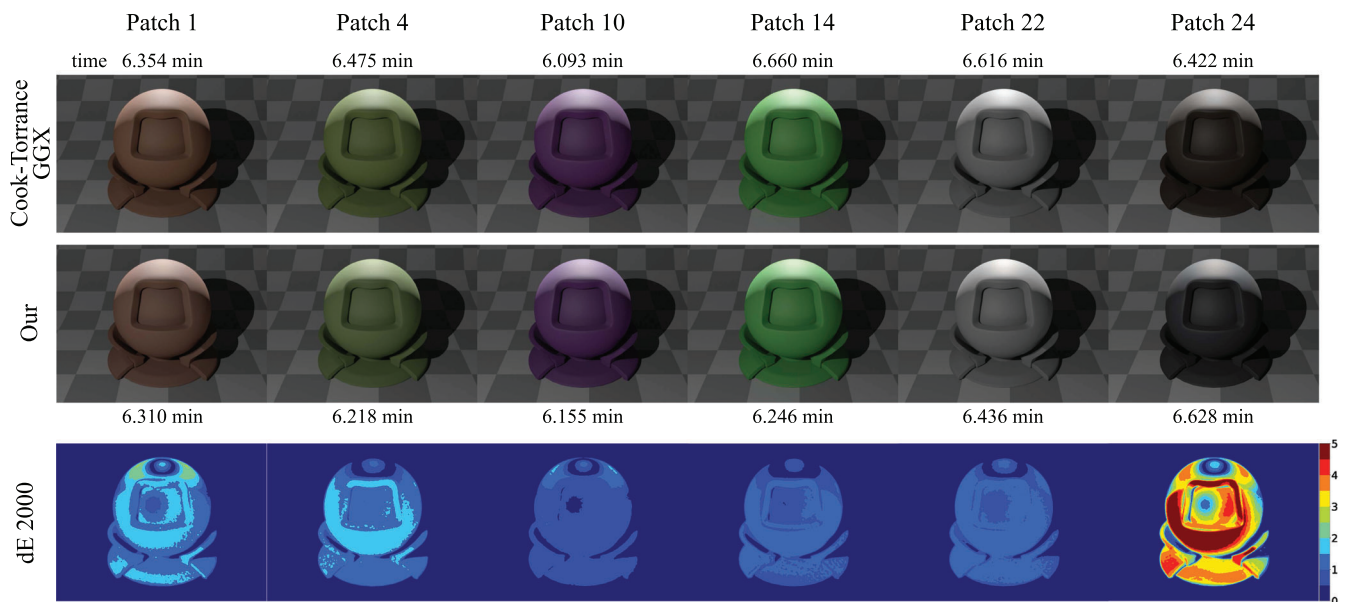
Similar fitting results are obtained for all ColorChecker patches. The results for six patches are shown in Table 2.

6.3. Renderings

To demonstrate the influence of the wavelength shifts on the object's appearance, we generated renderings with the Cook–Torrance
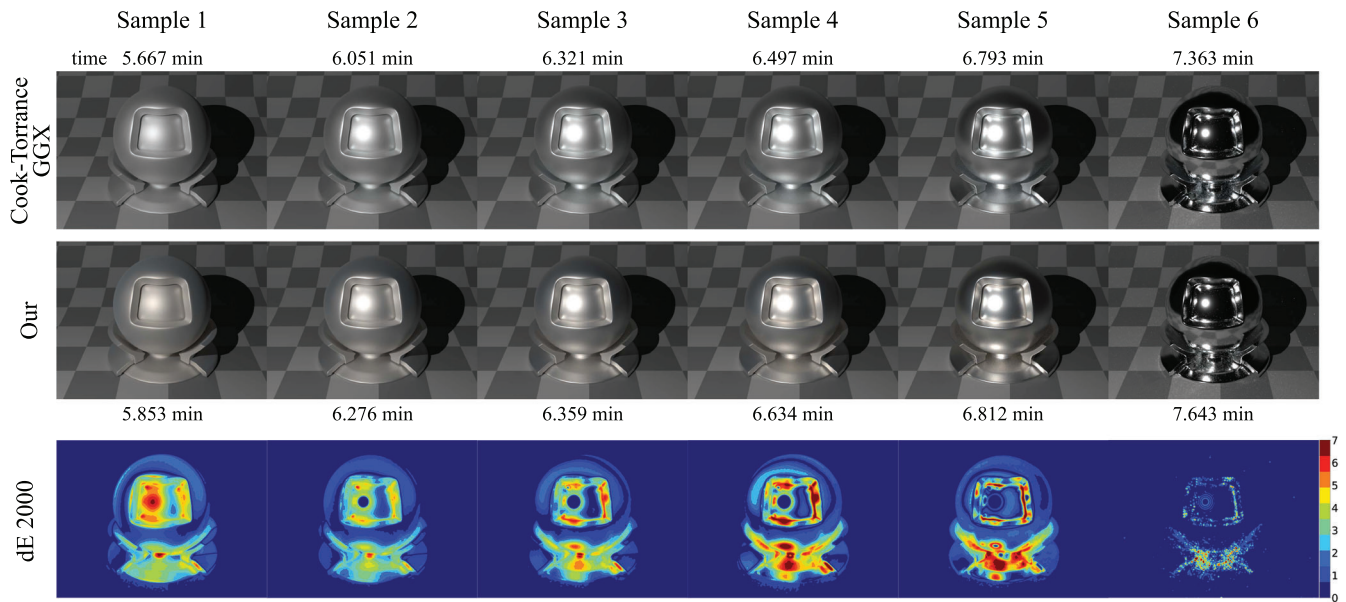
(a) Aluminum samples.

(b) ColorChecker patches.

Figure 14: *Renderings computed with Mitsuba 2 [NDVZJ19] and the fitted BRDFs of aluminium samples (a) and ColorChecker patches (b). For both conductors and dielectrics, clear differences between the Cook–Torrance and our model can be observed, as confirmed by large Delta E 2000 values. Note the different scales of the colourbars.*

and our model of the aluminium samples and the ColorChecker patches. We used Mitsuba 2 [NDVZJ19] with the plugins *roughconductor* and *roughdielectric* extended by the shift function as in Equations (7) and (8). Further, we used a modified version of the *matpreview* scene provided by Mitsuba, where a spotlight replaces the environment map. Figure 14 presents renderings of six aluminium samples and six ColorChecker patches along with the corresponding render times, as well as the dE00 image between the renderings computed with the Cook–Torrance and our model.

For the aluminium samples (Figure 14a), the Cook–Torrance model leads to a homogeneous, greyish appearance. On the contrary, with our model, the object is tinted yellowish and towards the edges bluish. This effect can be well-observed on rougher surfaces, such as Sample 1. The dE00 images demonstrate that the overall differences between the renderings diminish with increasing smoothness. However, in the bottom part of the *matpreview* object, the dE00 actually increases, probably due to multiple reflections. In our opinion, our model leads to a more natural, realistic look, while the object appears more synthetic with the Cook–Torrance model.

For the ColorChecker patches (Figure 14b), the differences between the renderings are more subtle but still prominent. The renderings demonstrate that the Cook–Torrance model leads to a slightly reddish-tinted diffuse reflection for all patches. This effect is particularly strong at Patch 24 with dE00s as high as five.

The render times of the Cook–Torrance and our model are practically the same. Only for conductors, an increase of up to 3% is observed. The simplicity of the model, accompanied by the low computational costs, is huge benefits compared to current diffraction models and, consequently, enables its use in real-time applications.

7. Conclusions

Our experimental investigation of light interaction with rough surfaces not only gives a better understanding of scattering phenomena but also allows us to describe them in a simple way. In this work, we combined different measurement modalities to thoroughly analyse some underlying phenomena that significantly influence the material's appearance. This unique dataset will be made available with the paper publication and consists of in-plane BRDFs, micro-geometries, macro photos and scatter simulations of eight aluminium samples with varying roughness.

Based on the analysis of the experimental results, we posited the theory that single reflections, pre-dominately in the forward scattering, leading to a linear wavelength shift towards long wavelengths, thus to a reddish appearance. Contrary, multiple scattering, predominately in back-scattering, leads to a linear shift towards short wavelengths, hence a bluish appearance. We conclude that both phenomena are caused by diffraction. We observed that these linear wavelength shifts significantly impact the appearance of rough conductors. It also influences, even if less prominently, the appearance of dielectrics. Our conclusions are in agreement with all different measured data modalities. Furthermore, simulations using wave and geometric optics back our claims.

These are novel insights for the computer graphics community, and breaking down the scattering phenomena allows for considering diffraction effects in a simplified manner. This is well-demonstrated by the introduced diffraction model, where the Cook–Torrance model is extended by the shift function to account for diffraction. The simple approach outperforms the Cook–Torrance model for all tested dielectrics and conductors at nearly no extra computational costs. The provided renderings further demonstrate the high impact of the wavelength shifts on the visual appearance.

Even though we could adequately fit the data from each sample with the proposed local and global models, it is not yet clear how the diffraction phenomena relate to roughness parameters. More research in this direction may lead to a general model based on surface roughness. Finally, we would like to look closely at the non-conformity of the off-specular peak for the simulations with wave and geometric optics.

References

[BGM*04] BUHLERT M., GARTNER M., MODREANU M., JITIANU A., GAVRILA R., AWAD A., PLATH P.: Characterisation of electropolished aluminium surfaces. *Galvanotechnik 95*, 7 (2004), 1629–1634.

[BNM15] BUTLER S. D., NAUYOKS S. E., MARCINIAK M. A.: Experimental measurement and analysis of wavelength-dependent properties of the BRDF. In *Proceedings of the Imaging Spectrometry XX* (2015), vol. 9611, SPIE, pp. 78–92.

[BS87] BECKMANN P., SPIZZICHINO A.: *The Scattering of Electromagnetic Waves from Rough Surfaces*. Artech House, Inc., Norwood, 1987.

[BSH12] BAGHER M. M., SOLER C., HOLZSCHUCH N.: Accurate fitting of measured reflectances using a shifted gamma microfacet distribution. *Computer Graphics Forum 31*, 4 (2012), 1509–1518.

[Bur12] BURLEY B.: Physically-based shading at disney. In *SIGGRAPH'12: Proceedings of the ACM SIGGRAPH 2012 Courses* (New York, NY, USA, 2012), Association for Computing Machinery. https://doi.org/10.1145/2343483.2343493

[CJZ79] CHURCH E., JENKINSON H., ZAVADA J.: Relationship between surface scattering and microtopographic features. *Optical Engineering 18*, 2 (1979), 182125.

[CMF18] CLAUSEN O., MARROQUIM R., FUHRMANN A.: Acquisition and validation of spectral ground truth data for predictive rendering of rough surfaces. *Computer Graphics Forum 37*, 4 (2018), 1–12.

[CMFW19] CLAUSEN O., MARROQUIM R., FUHRMANN A., WEIGAND H.: What is the Reddening Effect and does it really exist? In *Proceedings of the Workshop on Material Appearance Modeling* (2019), R. Klein and H. Rushmeier (Eds.), The Eurographics Association. http://doi.org/10.2312/mam.20191309

[CSC*16] CHENG F., SU P.-H., CHOI J., GWO S., LI X., SHIH C.-K.: Epitaxial growth of atomically smooth aluminum on silicon and its intrinsic optical properties. *ACS Nano 10*, 11 (2016), 9852–9860.

[CT81] COOK R. L., TORRANCE K. E.: A reflectance model for computer graphics. *SIGGRAPH Comput. Graph. 15*, 3 (Aug. 1981), 307–316. URL: https://doi.org/10.1145/965161.806819,

[DJ18] DUPUY J., JAKOB W.: An adaptive parameterization for efficient material acquisition and rendering. *ACM Transactions on Graphics 37*, 6 (Dec. 2018). https://doi.org/10.1145/3272127.3275059

[DSM*15] DURELL C., SCHARPF D., MCKEE G., L'HEUREUX M., GEORGIEV G., OBEIN G., COOKSEY C.: Creation and validation of Spectralon PTFE BRDF targets and standards. In *Sensors, Systems, and Next-Generation Satellites XIX* (2015), R. Meynart, S. P. Neeck and H. Shimoda (Eds.), vol. 9639, International Society for Optics and Photonics, SPIE, pp. 96391D. https://doi.org/10.1117/12.2195503

[DWMG16] DONG Z., WALTER B., MARSCHNER S., GREENBERG D. P.: Predicting appearance from measured microgeometry of metal surfaces. *ACM Transactions on Graphics 35*, 1 (Dec. 2016). https://doi.org/10.1145/2815618

[FV14] FILIP J., VÁVRA R.: Template-based sampling of anisotropic BRDFs. *Computer Graphics Forum 33*, 7 (2014), 91–99.

[FVH14] FILIP J., VÁVRA R., HAVLÍCEK M.: Effective acquisition of dense anisotropic BRDF. In *Proceedings of the 2014 22nd International Conference on Pattern Recognition* (2014), IEEE, pp. 2047–2052.

[GGG*16] GUARNERA D., GUARNERA G., GHOSH A., DENK C., GLENCROSS M.: BRDF representation and acquisition. *Computer Graphics Forum 35*, 2 (2016), 625–650.

[HP17] HOLZSCHUCH N., PACANOWSKI R.: A two-scale microfacet reflectance model combining reflection and diffraction. *ACM Transactions on Graphics 36*, 4 (July 2017). https://doi.org/10.1145/3072959.3073621

[HTSG91] HE X. D., TORRANCE K. E., SILLION F. X., GREENBERG D. P.: A comprehensive physical model for light reflection. *ACM SIGGRAPH Computer Graphics 25*, 4 (July 1991), 175–186.

[KHC11] KRYWONOS A., HARVEY J. E., CHOI N.: Linear systems formulation of scattering theory for rough surfaces with arbitrary incident and scattering angles. *JOSA A 28*, 6 (June 2011), 1121–1138.

[LD18] LEVESQUE M. P., DISSANSKA M.: Correction of the calibration measurement by taking into account the Spectralon spectropolarimetric BRDF model. In *Reflection, Scattering, and Diffraction from Surfaces VI* (2018), L. M. Hanssen (Ed.), vol. *10750*, International Society for Optics and Photonics, SPIE, pp. 107500H. https://doi.org/10.1117/12.2323603

[LKYU12] LÖW J., KRONANDER J., YNNERMAN A., UNGER J.: Brdf models for accurate and efficient rendering of glossy surfaces. *ACM Transactions on Graphics 31*, 1 (Feb. 2012). https://doi.org/10.1145/2077341.2077350

[lmf] LMFIT: Non-linear least-square minimization and curve-fitting for Python. (2021). https://zenodo.org/record/4516651

[Möl88] MÖLLER K. D.: Optics. University Science Books, New York. 1988.

[MPBM03] MATUSIK W., PFISTER H., BRAND M., MCMILLAN L.: A data-driven reflectance model. *ACM Transactions on Graphics 22*, 3 (July 2003), 759–769.

[MPL16] MARTIN P. LEVESQUE M. D.: *Measurement and modeling of the Spectralon spectro-polarimetric bidirectional reflectance distribution function (BRDF)*. Tech. Rep., DRDC - Valcartier Research Center, 2016.

[NDM05] NGAN A., DURAND F., MATUSIK W.: Experimental analysis of BRDF models. In *Proceedings of the 16th Rendering Techniques*, vol. 2.

[NDVZJ19] NIMIER-DAVID M., VICINI D., ZELTNER T., JAKOB W.: Mitsuba 2: A retargetable forward and inverse renderer. *ACM Transactions on Graphics 38*, 6 (Nov. 2019). https://doi.org/10.1145/3355089.3356498

[OM87] O'DONNELL K., MENDEZ E.: Experimental study of scattering from characterized random surfaces. *JOSA A 4*, 7 (1987), 1194–1205.

[Ric51] RICE S. O.: Reflection of electromagnetic waves from slightly rough surfaces. *Communications on Pure and Applied Mathematics 4*, 2-3 (1951), 351–378.

[SDC*11] SCHRÖDER S., DUPARRÉ A., CORIAND L., TÜNNERMANN A., PENALVER D. H., HARVEY J. E.: Modeling of light scattering in different regimes of surface roughness. *Optics Express 19*, 10 (May 2011), 9820–9835.

[SY21] STEINBERG S., YAN L.-Q.: A generic framework for physical light transport. *ACM Transactions on Graphics 40*, 4 (July 2021). https://doi.org/10.1145/3450626.3459791

[TR75] TROWBRIDGE T. S., REITZ K. P.: Average irregularity representation of a rough surface for ray reflection. *Journal of the Optical Society of America 65*, 5 (May 1975), 531–536.

[TS67] TORRANCE K. E., SPARROW E. M.: Theory for off-specular reflection from roughened surfaces. *Journal of the Optical Society of America 57*, 9 (Sep. 1967), 1105–1114.

[WGK14] WEINMANN M., GALL J., KLEIN R.: Material classification based on training data synthesized using a BTF database. In *Proceedings of the 13th European Conference on Computer Vision - ECCV 2014, Part III* (Zurich, Switzerland, 2014), Springer International Publishing, pp. 156–171.

[WMLT07] WALTER B., MARSCHNER S. R., LI H., TORRANCE K. E.: Microfacet models for refraction through rough surfaces. In *Rendering Techniques* (2007), J. Kautz and S. Pattanaik (Eds.), The Eurographics Association. http://doi.org/10.2312/EGWR/EGSR07/195-206

[WVJH17] WERNER S., VELINOV Z., JAKOB W., HULLIN M. B.: Scratch iridescence: Wave-optical rendering of diffractive surface structure. *ACM Transactions on Graphics 36*, 6 (Nov. 2017). https://doi.org/10.1145/3130800.3130840,

[YHW*18] YAN L.-Q., HAŠAN M., WALTER B., MARSCHNER S., RAMAMOORTHI R.: Rendering specular microgeometry with wave optics. *ACM Transactions on Graphics 37*, 4 (July 2018). https://doi.org/10.1145/3197517.3201351